

IMPROVING SHAPE SENSING OF AERONAUTICAL STRUCTURES WITH STRAIN PRE-EXTRAPOLATION AND SENSOR PLACEMENT OPTIMIZATION

Emiliano Del Priore¹, Luca Lampani¹

¹Sapienza Università di Roma, Dipartimento di Ingegneria Meccanica e Aerospaziale, Roma, 00184, Italia

Abstract

Shape sensing is a branch of Structural Health Monitoring that allows real-time reconstruction of a structure displacement field from discrete strain measurements. The inverse Finite Element Method (iFEM) is a highly effective approach for this purpose. However, iFEM accuracy heavily relies on the number of installed sensors, which presents practical implementation and cost challenges. To mitigate these issues and achieve highly accurate results with significantly fewer sensors, iFEM is combined with Smoothing Element Analysis (SEA), a technique that allows the pre-extrapolation of the strain field across the entire structure from a limited number of measurement points. Effective SEA extrapolation across multiple load cases requires strategic sensor placement. This study proposes an optimization strategy using a multi-objective genetic algorithm to determine an optimal sensor layout for the combined use of SEA and iFEM. This approach aims to enhance SHM effectiveness for aeronautical structures such as stiffened panels under various operational scenarios. Results demonstrate significant improvements in monitoring capabilities with a reduced number of sensors, maintaining comparable accuracy to conventional iFEM.

Keywords: structural health monitoring; shape sensing; optimal sensor placement; inverse finite element method.

1. Introduction

I

The in-service Structural Health Monitoring (SHM) of aircraft structures plays a key role in estimating their performance and integrity. By strategically deploying sensors, a Structural Health Monitoring system collects crucial data about the structure and its environment, enabling a comprehensive evaluation of the overall state of the system. SHM differs fundamentally from Non-Destructive Testing (NDT) by allowing real-time monitoring without human intervention [1].

Within the context of SHM, increasing research efforts have been put into the development of shape sensing techniques, which enable the real-time evaluation of the displacement field from discrete strain measurements. These methods allow continuous tracking of both static and dynamic responses, which can also be employed to evaluate stresses across the structure. Among the various shape sensing techniques, the inverse Finite Element Method (iFEM) [2] has emerged as a prominent approach. iFEM employs a weighted least-squares variational principle to reconstruct the displacement field by discretizing the structural domain into inverse finite elements and minimizing the error between analytical and experimental strain measures. This method is particularly advantageous for monitoring structures under stochastic loading conditions, as it does not require knowledge of the material properties or applied loads [3]. In recent years, iFEM has been applied in both numerical and experimental shape-sensing analyses for various complex case studies, including wing boxes [4], stiffened panels [5] and spaceborne antennas [6]. The potential of iFEM extends beyond linear problems as it also includes scenarios involving large deformations. For example, such an approach has been applied to monitor the deflection of thin laminated plates in post-buckling conditions [7]. The inverse Finite Element Method has also been applied successfully in the context of damage diagnosis, proving to be a valuable tool for identifying cracks [8], estimate their size [9] and growth [10].

Despite its benefits, the accuracy of iFEM is heavily dependent on the number of sensors, posing a challenge in terms of cost and practicality. To address this limitation, strain interpolation and extrapolation techniques, such as Smoothing Element Analysis (SEA) [11], have been introduced. SEA relies on a variational principle and discretizes the geometry into a triangular mesh to produce a continuous description of the strain field from a limited number of sensors [12]. This approach allows

the use of dense meshes in iFEM, ensuring high accuracy by providing virtual measurement information for each element. As an example, Oboe et al. [13] employed SEA in conjunction with iFEM to the shape sensing problem of a plate subjected to a compressive load. However, optimizing sensor placement becomes crucial to enhance the effectiveness of SEA, particularly under various loading conditions [14].

This study proposes an optimization strategy using the Non-dominated Sorting Genetic Algorithm II (NSGA-II) [15] to find an optimal sensor layout capable of accurately reconstructing deformations under multiple loading conditions. In this process, Smoothing Element Analysis is employed to pre-extrapolate strain data, which serves as input for the inverse Finite Element Method. Each sensor layout is evaluated based on the error between the iFEM reconstructed displacement field and the reference solution. By integrating SEA with optimal sensor placement within the iFEM framework, the method aims to enhance Structural Health Monitoring system capabilities for aeronautical structures, such as hat-stiffened panels, under various operational scenarios. Results from this combined approach are compared those of conventional iFEM to illustrate its effectiveness, indicating a significant improvement in monitoring capabilities by using a reduced number of sensors while maintaining a similar accuracy.

2. Theoretical Background

I

2.1 Inverse Finite Element Method (iFEM)

The inverse Finite Element Method (iFEM) reconstructs the displacement field of the system by discretizing the structural domain with a set of inverse finite elements and minimizing an error functional. Within each element, such functional Φ^e is defined as the weighted least-squares difference between the analytic strain measures and the corresponding experimental ones obtained from in-situ strain sensors placed on the structure. For a shell element based on the First Order Shear Theory Φ^e is expressed as [16]

$$\mathbf{\Phi}^e = w_m \|(\mathbf{e}_i - \mathbf{e}_i^{\varepsilon})\|^2 + w_b (2h)^2 \|(\mathbf{k}_i - \mathbf{k}_i^{\varepsilon})\|^2 + w_s \|(\mathbf{g}_i - \mathbf{g}_i^{\varepsilon})\|^2$$
(1)

In Equation 1 e, k and g are the membrane, bending, and transverse shear strains respectively, the superscript ε is used to denote the values measured from a strain sensor and w_m , w_b and w_s are appropriate weighting constants. In general, these weights are set to unity but, if an element lacks experimental strain data, they are assigned a small value, e.g., 10^{-4} . Given a structure equipped with a set of surface mounted strain sensors as shown in Figure 1, the experimental membrane and curvature strains at the i-th measurement (i=1,...,n) point can be derived as follows (the superscripts + and - refer to the quantities corresponding to the top and bottom surface, respectively)

$$\boldsymbol{e}_{i}^{\varepsilon} = \frac{1}{2} \begin{cases} \varepsilon_{xx}^{+} + \varepsilon_{xx}^{-} \\ \varepsilon_{yy}^{+} + \varepsilon_{yy}^{-} \\ \gamma_{xy}^{+} + \gamma_{xy}^{-} \end{cases} \qquad \boldsymbol{k}_{i}^{\varepsilon} = \frac{1}{2h} \begin{cases} \varepsilon_{xx}^{+} - \varepsilon_{xx}^{-} \\ \varepsilon_{yy}^{+} - \varepsilon_{yy}^{-} \\ \gamma_{xy}^{+} - \gamma_{xy}^{-} \end{cases}$$
 (2)

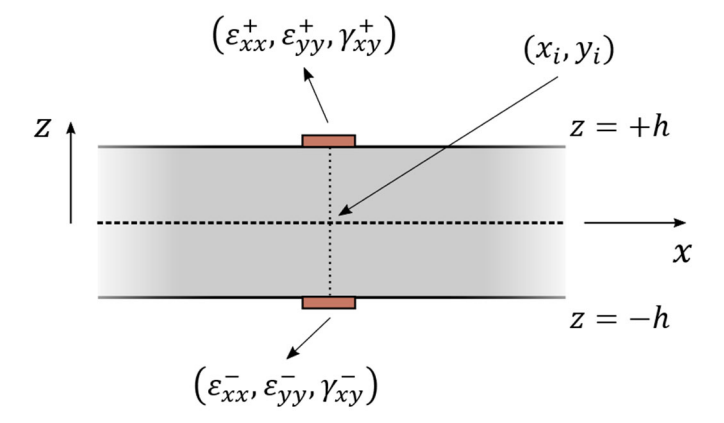


Figure 1: Discrete surface strains at i-th measurement point

The kinematic variables inside each element (3 translations and 2 rotations) can be interpolated by

means of a set of shape functions

$$\left[u \ v \ w \ \theta_x \ \theta_y\right]^T = N^e u^e \tag{3}$$

In Equation (3), N^e denotes the matrix of shape functions, and u^e is a vector which collects the nodal degrees of freedom of the element. Next, the strain components can be expressed as the product between the matrices \mathbf{B}_m , \mathbf{B}_b , and \mathbf{B}_s containing the derivatives of the shape functions, and the element nodal displacements \mathbf{u}^e .

$$e(u^e) = B_m u^e \qquad k(u^e) = B_b u^e \qquad g(u^e) = B_s u^e \tag{4}$$

By inserting Equation (4) into the functional of Equation (1) and minimizing it with respect to u^e one obtains a linear system

$$\frac{\partial \Phi(u^e)}{\partial u^e} = 0 \quad \rightarrow \quad K^e u^e = F^e \tag{5}$$

With

Ī

$$\mathbf{K}^{e} = \int_{A_{s}} \left(w_{m} \mathbf{B}^{mT} \mathbf{B}^{m} + (2h)^{2} \mathbf{B}^{b}^{T} \mathbf{B}^{b} + w_{s} \mathbf{B}^{sT} \mathbf{B}^{s} \right) dA$$
 (6)

$$\boldsymbol{F}^{e} = \frac{1}{n} \int_{A_{e}} \sum_{i=1}^{n} \left(w_{m} \boldsymbol{B}^{mT} \boldsymbol{e}_{i}^{\varepsilon} + (2h)^{2} \boldsymbol{B}^{bT} \boldsymbol{k}_{i}^{\varepsilon} + w_{s} \boldsymbol{B}^{sT} \boldsymbol{g}_{i}^{\varepsilon} \right) dA$$
 (7)

After a standard assembly process of a finite element method, a linear system of the equations is built, with the nodal displacements U of the whole structure as unknowns, as displayed in Equation (8).

$$KU = F \tag{8}$$

where K is a matrix depending on the shape functions and strain-sensor locations, whereas F is a vector which depends on the measured data [17]. Since the formulation relies solely on strain-displacement relations, it enables the reconstruction of both static and dynamic responses without requiring any a priori knowledge of the material properties of the structure. Moreover, the algorithm speed makes it suitable for real-time applications.

2.2 Smoothing Element Analysis (SEA)

The accuracy of the inverse Finite Element Method is significantly influenced by the number of sensors used. Installing a multitude of sensors to achieve low error can be excessively costly and impractical in the aeronautical industry. Therefore, it can be beneficial to employ pre-extrapolation techniques to obtain a continuous description of the input strain field from a reduced number of sensors. One such technique is Smoothing Element Analysis (SEA), which was initially proposed for finite element stress recovery and a posteriori error estimation. This robust computational technique effectively extrapolates a scalar quantity, such as a strain component, measured at discrete locations within the structure. It generates a smoothed C1-continuous field with C0-continuous derivatives. The numerical formulation of SEA relies on a variational principle employing a penalized-discrete-least-squares (PDLS) functional. The algorithm adopts a finite element approach, in which the geometry is discretized into a triangular mesh and within each element the functional is defined as

$$\Psi^{e} = \frac{1}{n} \sum_{i=1}^{n} \left(\varepsilon(\mathbf{x}_{i}) - \varepsilon_{i}^{h} \right)^{2} + \alpha \int_{S} \left(\left(\varepsilon_{,x} - \kappa_{x} \right)^{2} + \left(\varepsilon_{,y} - \kappa_{y} \right)^{2} \right) dS + \beta S \int_{S} \left(\left(\kappa_{x,x} \right)^{2} + \left(\kappa_{y,y} \right)^{2} + \frac{1}{2} \left(\kappa_{x,y} + \kappa_{y,x} \right)^{2} \right) dS$$

$$(9)$$

where n is the total number of measurements within the element; ε_i^h is a general measured strain and

 $\varepsilon(x_i)$ denotes the corresponding strain after the smoothing process; $(\cdot)_{,x}$ and $(\cdot)_{,y}$ represent the partial derivative operator with respect to x and y; κ_x and κ_y are the analytical counterpart of the partial derivatives of the experimental strain along directions x and y respectively; α and β are dimensionless constants. A triangular element of the SEA mesh with its corresponding nodal degrees of freedom is displayed in Figure 2. The scalar field within an element is interpolated using suitable shape functions, and the contribution from all the elements are assembled to compute the total error functional Ψ . Minimizing Ψ with respect to the nodal dofs and solving the resultant linear algebraic equations yields the nodal components of the smoothed scalar field, i.e., a strain field component, and its derivatives in each node.

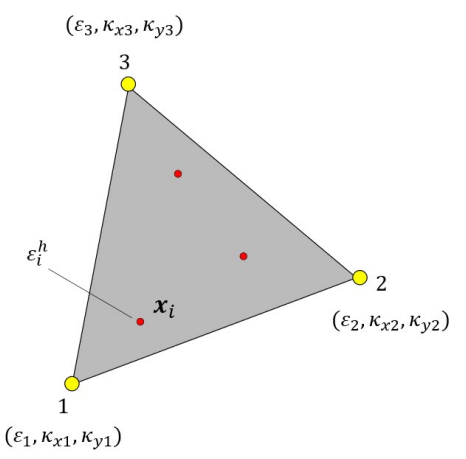


Figure 2: Triangolar smoothing element with its nodal dofs.

2.3 Multi-objective Genetic Algorithm

I

A Genetic Algorithm (GA) is a heuristic optimization method inspired by the principles of natural selection. A GA operates on a population where each individual represents a potential solution to the optimization problem. This population, usually initialized randomly, evolves over time, with fitter solutions becoming more prevalent. GA uses two main operators to generate new solutions: crossover and mutation [18]. In the crossover process, two parent individuals are combined to produce an offspring, favoring fitter individuals through a selection operator. This operation integrates superior genes into the population, driving convergence towards an optimal solution. Mutation introduces random changes, maintaining genetic diversity and helping to escape local optima.

For multi-objective optimization problems, achieving a solution that is optimal for every objective is often impossible. Instead, a Multi-objective Genetic Algorithm (MOGA) seeks a set of Pareto-optimal solutions. NSGA-II is a specific version of MOGA that operates similarly to a single-objective GA but includes specific selection operations [19]:

- Fast non-dominated sorting approach: The population is sorted into different non-dominated fronts. Individuals in the first non-dominated front are identified, and their rank is set to 1. The remaining individuals, excluding those with rank 1, continue to be sorted using the same procedure until all fronts are identified. An example of population in the solution space organized in non-dominated fronts is displayed in Figure 3.
- Crowding Distance Assignment: Individuals with the same rank are arranged based on crowding distance, which represents the average distance in the objective space between a solution and its neighboring solutions on the same front.
- Selection operator: Binary tournament selection is employed to choose parents. Two individuals are randomly selected from the population, and if their ranks differ, the one with the smaller rank is chosen. If their ranks are the same, the individual with a larger crowding distance is selected. This method ensures a more even distribution of solutions along the Pareto front, preventing overcrowding in specific regions.

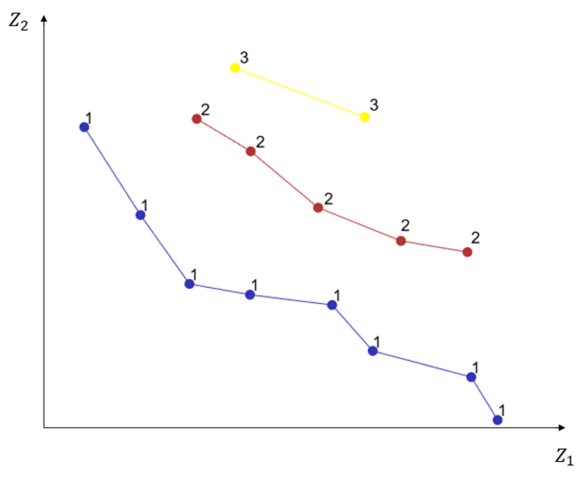


Figure 3: Example of solution in the objective space (two-objectives Z_1 and Z_2); points marked with the same color belong to the same non-dominated front.

2.4 Proposed Methodology

I

In this study, we utilize Smoothing Element Analysis to pre-extrapolate the strain field, which serves as input for the inverse Finite Element Method. This smoothing process generates a continuous description of the strain field, enabling the application of iFEM on a fine mesh. To ensure accurate reconstruction, we optimize sensor placement using a genetic algorithm. Given that structures usually experience various loading conditions, a multi-objective optimization based on multiple operational scenarios is necessary. Therefore, we employ the Non-dominated Sorting Genetic Algorithm (NSGA-II) for this purpose.

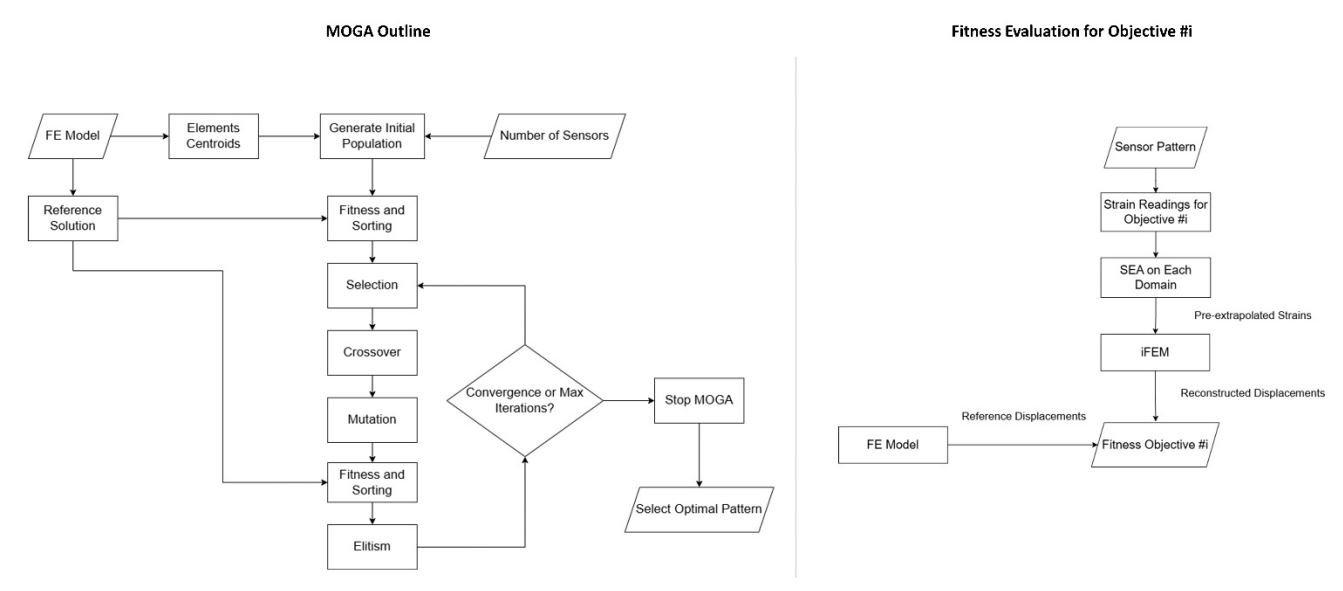


Figure 4: Flowchart of the optimization algorithm (left) and of the process to evaluate the fitness of the i-th objective (right).

The optimization procedure is outlined in the following paragraph and in the flowchart of Figure 4. A Finite Element (FE) model of the structure generates discrete strain data (simulating real-world sensor readings) and provides a reference solution for evaluating the accuracy of results obtained from the shape sensing technique. Potential sensor locations for the optimization process are chosen from the centroids of 4-node quadrilateral shell elements of the same FE mesh. Once the number of sensors to be installed is determined, each individual in the population is represented as an array of Cartesian coordinates corresponding to the sensor layout. The number of individuals is denoted as N_{pop} . For each individual in the population, SEA pre-extrapolates each component of the membrane strains and bending curvatures. These are used as input for the inverse Finite Element Method to reconstruct the displacement field. Since the case studies involve stiffened panels, and strain fields at stiffener-panel junctions are generally discontinuous, SEA is applied in separate, independent domains to avoid unphysical smoothing across these junctions [20]. In Figure 5, an example of a hat-stiffened panel is

divided into six independent smoothing domains each depicted in a different color. Within each domain, strain resultants are defined relative to a convenient coordinate system, and these strain components are smoothed independently. This process produces a continuous description of the strain field, enabling the application of iFEM on a fine mesh for the whole structure.

The accuracy of the reconstructed solution for each individual is evaluated using the root mean square error (rmse) between the iFEM reconstructed displacement magnitude and the reference solution:

$$f_r = rmse(\boldsymbol{u_r}^{iFEM}, \boldsymbol{u_r}^{ref}) \quad (r = 1, ..., N_{obj})$$
 (10)

Through this procedure the fitness of the whole population can be evaluated.

I

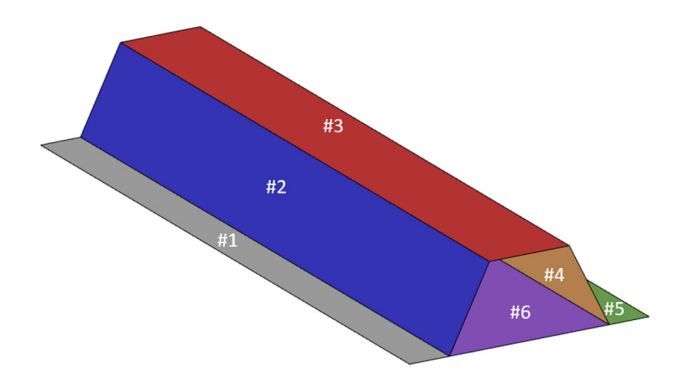


Figure 5: An example of hat-stiffened panel with each smoothing domain depicted in a different color.

For each iteration of the genetic algorithm, crossover and mutation are applied until convergence to a set of Pareto-optimal solutions is achieved. These processes can occur with a probability denoted as p_{cross} and p_{mut} respectively. This study uses a uniform crossover, where each gene of an offspring is randomly selected from one of the parents with equal probability. Figure 6 (a) illustrates an example of such a crossover on a square plate. The blue and red dot patterns on the left represent Parent 1 and Parent 2, respectively. Following the crossover, the two resulting children inherit some sensor positions from Parent 1 (blue dots) and the remaining positions from Parent 2 (red dots). Some offsprings may undergo a mutation process. In this study, mutation involves changing the positions of n_{mut} random sensors in the individual pattern to other random positions among the set of centroids in the FE model. An example of such process is shown Figure 6 (b)): the two circled sensors of the individual on the left are randomly chosen to undergo the mutation process; on the right, the individual after mutation with the purple dots indicating the new positions of the two mutated sensors.

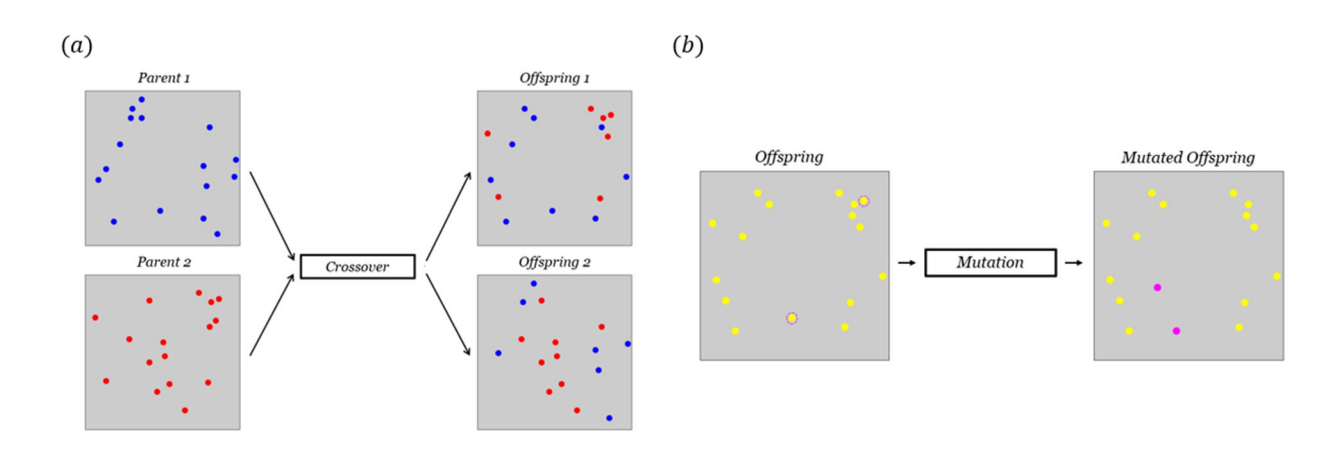


Figure 6: Uniform crossover (a) and mutation process (b).

At the end of the mutation process, elitism is applied to form the new population for reproduction, keeping only the best N_{pop} individuals among parents, offsprings, and mutated individuals. A ranking

is needed to choose the best N_{pop} solutions, and thus non-dominated sorting and crowding distance are employed. The use of elitism ensures that there is no loss of good genes between generations, leading to a monotonic convergence to the optimal solution.

3. Results

I

3.1 Case Study

The case study involves a rectangular plate reinforced with three equally spaced hat-stiffeners. Such a structure is assumed to be made of an isotropic material with properties similar to an aluminum alloy $(E=70~GPa,~v=0.3,~\rho=2700~kg/m^3)$. The geometric dimensions of the system are displayed in Figure 7 (a)-(c), and Table 1. The panel is constrained along the transverse sides (highlighted in red in Figure 7 (a)) to be simply supported, which restricts the three translational degrees of freedom u, v, and w. It should be noted that the constraints are applied only to the plate and not to the stiffeners. The longitudinal sides are left free to move.

This system is subjected to two different static loading conditions. The first condition is an upward uniform pressure load $p_1=1000~Pa$ applied to the plate to which the three hat-stiffeners are bonded. The second condition is a pressure load given by $p_2=k\sin\left(\frac{\pi X}{L_1}\right)\cos\left(\frac{\pi Y}{L_2}\right)$ with k=1000~Pa applied to the plate to which the three hat-stiffeners are bonded. These load conditions are chosen merely as examples and are not intended to simulate the actual loading conditions of the structure. Their purpose is solely to demonstrate the effectiveness of the entire process in the presence of relatively complex displacement fields.

Static analyses are performed using the commercial software MSC Nastran to obtain the reference displacement field for each loading scenario. The mesh used in the FE analysis is shown in Figure 7 (a) and consists of 2772 four-node shell elements. The centroids of these elements are extracted to represent potential sensor locations for the optimization process. For each sensor pattern, the strains at these points are extracted to be used in the SEA smoothing process. The mesh used by SEA is shown in Figure 1(b): the entire structure is divided into 20 subdomains, each with its own triangular mesh, where the pre-extrapolation process is independently conducted. Once the strain field is pre-extrapolated, the same FE reference mesh (the one displayed in Figure 7 (a)) is used by the inverse Finite Element Method to perform the shape sensing.

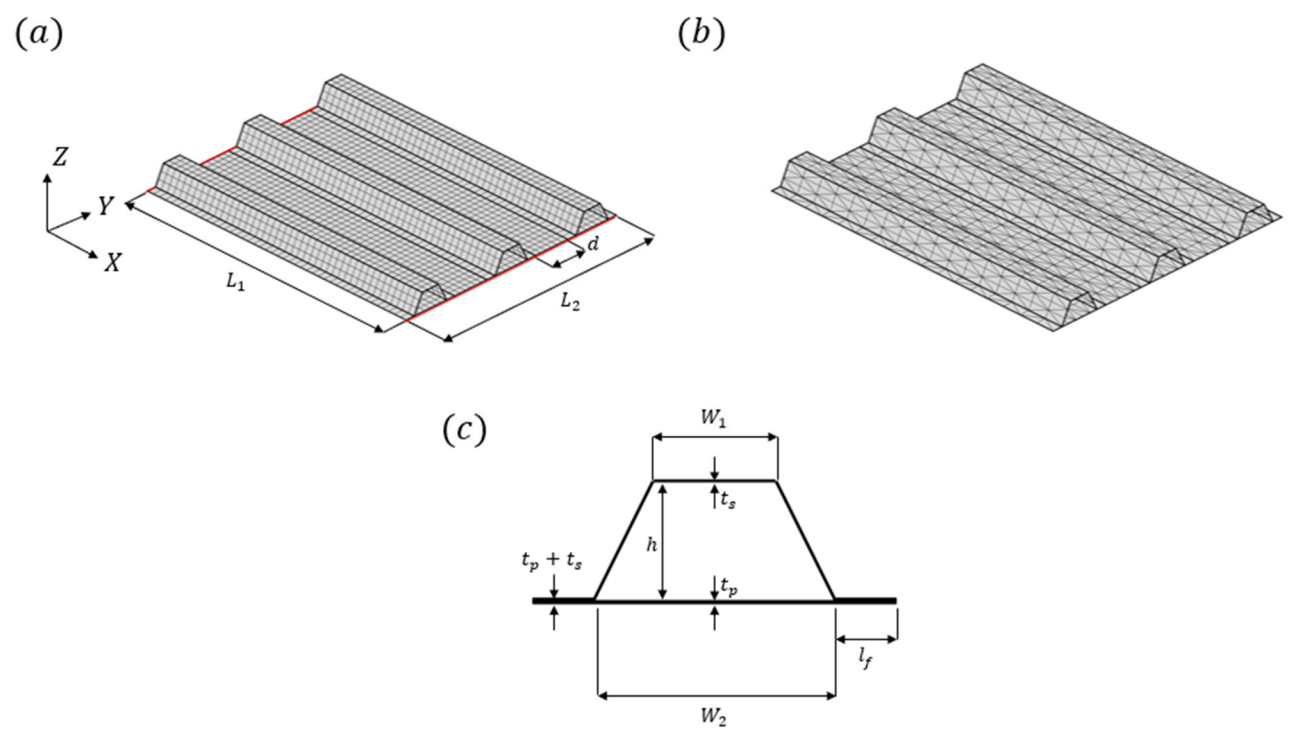


Figure 7: Four-nodes quadrilateral shell elements mesh (a), triangular smoothing elements mesh (b), section of a hat-stiffener (c).

L_1	L_2	d	W_1	W_2	l_f	h	t_p	t_{s}
800 mm	650 mm	100 mm	50 mm	100 mm	25 mm	50 mm	2 <i>mm</i>	0.5~mm

Table 1: Geometric dimensions of the hat-stiffened panel

3.2 Optimization Results

I

The number of sensors to be placed on the structure, denoted as N_s , is determined beforehand. It is chosen to ensure that the measurement points are sufficient to achieve a low error level in the reconstruction. The number of measurement points is kept to a reasonable value, ensuring the benefit of pre-extrapolation. Therefore, the optimization goal is to find a set of Pareto optimal sensor positions. After testing multiple values of N_s to monitor the displacement field of the case studies, we selected 25 measurement points.

The multi-objective genetic algorithm was run with a population of $N_{pop}=100$ individuals for 100 iterations, achieving convergence by the end. The crossover and mutation probabilities were set at $p_{cross}=0.9$ and $p_{mut}=0.1$ respectively. The number of mutated genes was selected as $n_{mut}=2$, and the number of elites was equal to N_{pop} , thus selecting the top 100 individuals among parents, offspring, and mutants. The optimization process was repeated multiple times to account for the inherent randomness of the genetic algorithm. From all the runs, the final population exhibiting the best global fitness was selected to extract a single solution. The final population from which the sensor pattern is selected is shown in Figure 8. The graph illustrates the evolution of fitness values for the two objectives, comparing the initial population (blue dots) with the final population (red dots), demonstrating the effectiveness of the optimization process. It should be noted that the final population includes multiple elements located on the Pareto front that repeat, making it appear as though it consists of fewer individuals.

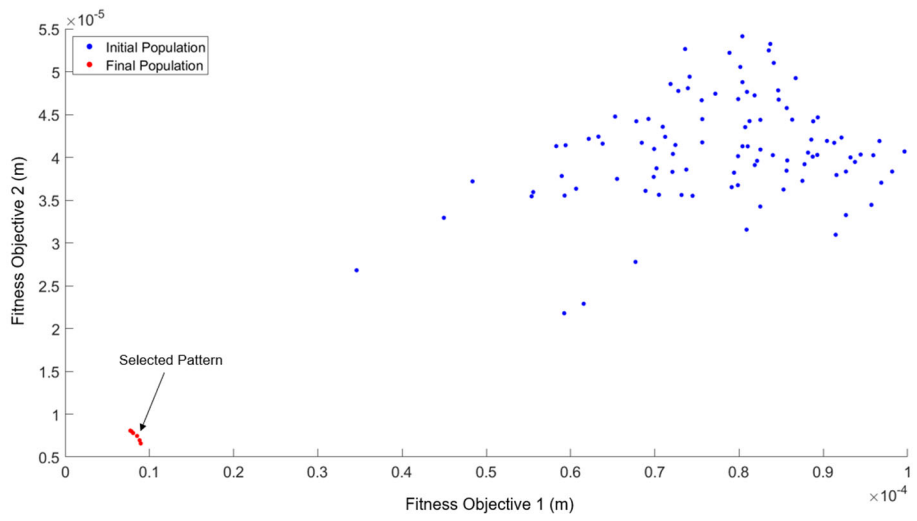
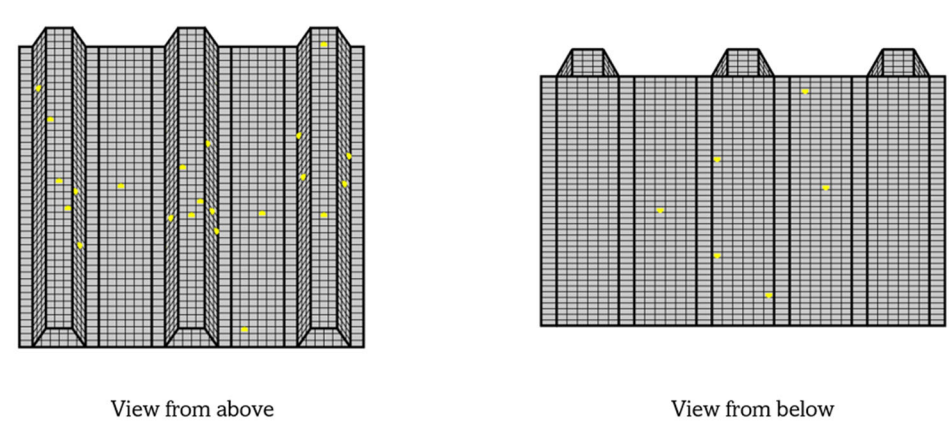


Figure 8: Evolution of the fitness between the initial population (blue dots) and the final one (red dots).

To choose an optimal individual from the final population, we selected a solution from the first Pareto front with well-balanced results for each objective (displayed in Figure 8). The chosen sensor arrangement is illustrated in Figure 9, with each measurement point displayed as a yellow dot. Theoretically each measurement point is associated with two strain rosettes—one for the top surface and another for the bottom one. However, in this case study, the inclined faces and the top face of the hat stiffeners deform mainly in membrane mode, while the rectangular plate and the flanges deform mainly in bending mode. Consequently, a single strain rosette can be used for each measurement point. For the membrane rosettes, it is indeed assumed that $\varepsilon_i^+ = \varepsilon_i^-$ (i = xx, yy, xy) and for the bending rosettes, it is assumed that $\varepsilon_i^+ = -\varepsilon_i^-$ (i = xx, yy, xy).

Using the optimal sensor pattern shown in Figure 9, the different components of the displacement field can be reconstructed and compared with the reference condition obtained from FE analysis.



I

Figure 9: Optimal sensor pattern for the hat-stiffened plate.

Figure 10 shows the Z direction displacement component, w, reconstructed with iFEM combined with SEA and MOGA, compared to the reference. This displacement component is shown because it is the predominant one, and only this is reported for brevity, but similar results are reported for u and v. As it can be seen, for both load conditions, the shape of the field is well captured, and the zones of maximum and minimum displacement are correctly identified. A slight asymmetry can be noted, which is due to the non-symmetric distribution of the chosen sensor pattern. This can be addressed during the design phase of the optimization process by imposing suitable constraints on the generation of individuals in the population. Additionally, observing the colorbars in Figure 10, the maximum displacement of the structure can be retrieved. For the case of uniform pressure load (Objective 1), the maximum vertical displacement produced by the reference FEM is about $0.2637 \ mm$, while that estimated by iFEM is $0.2547 \, mm$, with an error of approximately 3.5%. For the second loading condition (Objective 2), the maximum/minimum displacement is $\pm 0.13854 \, mm$ from the reference FEM, while the proposed method estimates a maximum of $0.13919 \, mm$ and a minimum of -0.13471 mm, with errors of 0.46% and 2.8%, respectively. Overall, the excellent shape sensing capabilities derived from the combination of iFEM with SEA and an appropriate choice of sensor pattern can be observed.

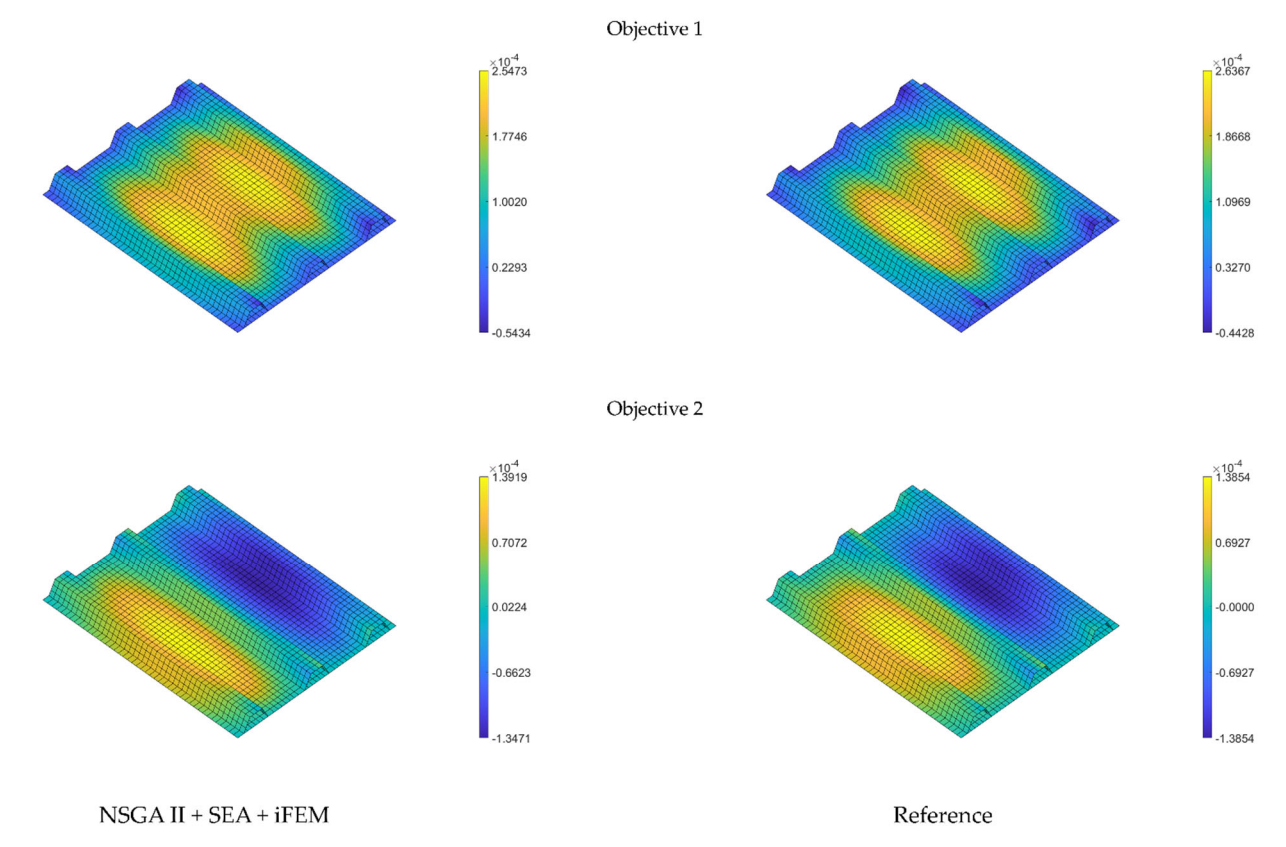


Figure 10: Comparison between reconstructed w displacement (in meters) for the proposed methodology and the reference FE solution for the two loading conditions.

Although the results obtained are valid for static loading conditions, the method can be extended to track dynamic responses. It is indeed possible to perform the optimization in such a way that the combination of SEA and iFEM can accurately reconstruct a set of the structure mode shapes. Since the dynamic response of a system can be represented as a weighted composition of the structure modes, the ability to accurately reconstruct these modes should also enable the adequate reconstruction of a dynamic response primarily influenced by the target modes.

3.3 Comparison with Conventional iFEM

I

To demonstrate the advantages of the proposed methodology over conventional iFEM (which does not use SEA and/or an optimized sensor pattern), a comparison of reconstruction capabilities between the two approaches is performed. Specifically, a comparison on how the maximum value of the displacement field magnitude is estimated relative to the reference solution, denoted as $\|\mathbf{U}\|_{max}^{iFEM}/\|\mathbf{U}\|_{max}^{ref}$, is drawn for both loading conditions. For conventional iFEM, this parameter is observed to vary as the mesh size decreases and therefore the number of elements, n_e , increases. In this process, it is assumed that each mesh element is equipped with a sensor, so n_e is equal to the number of installed sensors.

Figure 11 shows the trend of the ratio $\|\mathbf{U}\|_{max}^{iFEM}/\|\mathbf{U}\|_{max}^{ref}$ as the number of sensors increases, starting from a minimum of 60 up to a maximum of 2772 for each of the two objectives, represented by the blue curve. The errors can be quantified by observing how the curve deviates from the unit value (which would indicate a perfect estimation of the maximum displacement value). As can be seen, for both objectives, convergence is achieved with around 1000 elements, with errors of approximately 3.5% for the first load condition and close to 3.8% for the second. The dashed red line represents the solution obtained with the proposed methodology, using 25 sensors. Notably, comparable errors are achieved with the proposed method, significantly reducing the number of installed sensors. This demonstrates the effectiveness of the proposed approach.

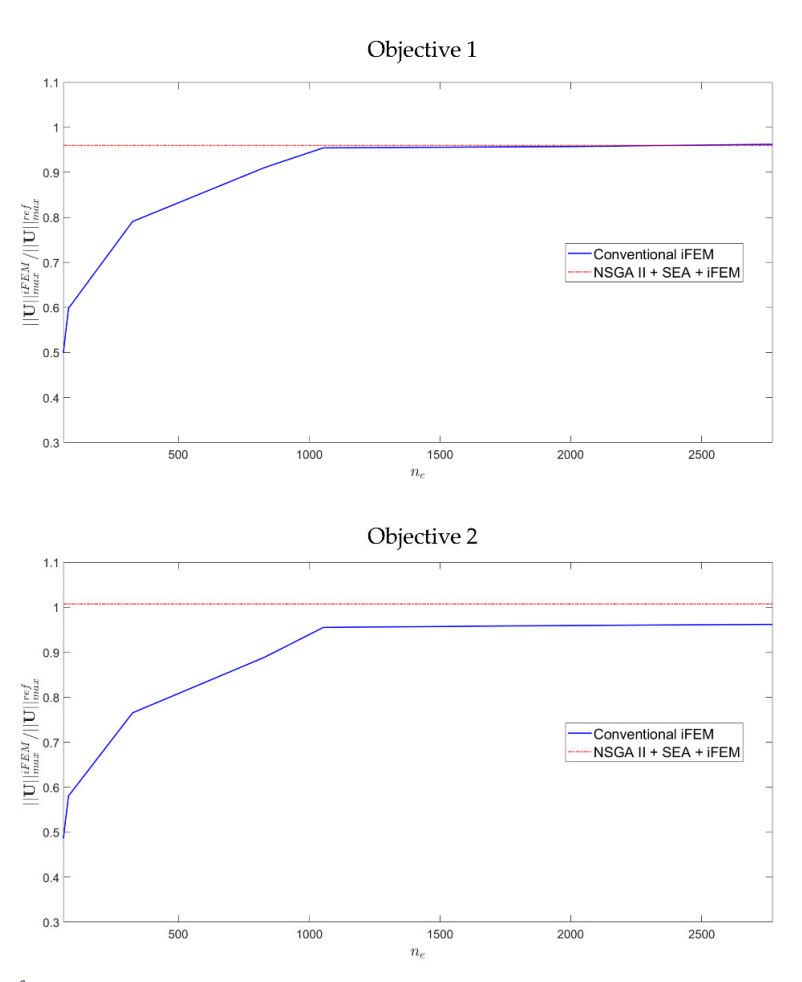


Figure 11: $\|U\|_{max}^{iFEM}/\|U\|_{max}^{ref}$ as the number of inverse elements increases for the conventional iFEM (blue curves) compared with the values from the proposed methodology (red dashed lines) for the two objectives.

4. Conclusions

I

This study introduces an innovative approach to the shape sensing problem of aeronautical structures by integrating Smoothing Element Analysis and Multi-objective Genetic Algorithms with the inverse Finite Element Method. The methodology was validated through numerical simulations on a hat-stiffened panel subjected to two different static pressure loads. The results indicate that the optimized sensor configuration, integrated with SEA, provides reconstruction accuracy comparable to conventional iFEM approaches but with far fewer sensors. This reduction in sensor count not only addresses practical and cost challenges but also maintains high monitoring fidelity, making it a viable solution for real-time Structural Health Monitoring (SHM) of complex structures. Although the method has been employed for static loading conditions, it can also be extended to dynamic loading scenarios. By optimizing the sensor placement to accurately reconstruct a set of natural modes of the structure, the combined SEA and iFEM approach can potentially ensure accurate dynamic response reconstruction.

5. Copyright Statement

The authors confirm that they, and/or their company or organization, hold copyright on all of the original material included in this paper. The authors also confirm that they have obtained permission, from the copyright holder of any third party material included in this paper, to publish it as part of their paper. The authors confirm that they give permission, or have obtained permission from the copyright holder of this paper, for the publication and distribution of this paper as part of the ICAS proceedings or as individual off-prints from the proceedings.

6. Acknowledgements

This work is framed within the Italian national project "MOST- Spoke 1 - AIR MOBILITY - WP5" which studies innovative solutions for next-generation green aircrafts.

References

- [1] A. Güemes, SHM Technologies and Applications in Aircraft Structures, 5th Int. Symp. NDT Aerosp. (2013) 13–15.
- [2] A. Kefal, E. Oterkus, A. Tessler, J.L. Spangler, A quadrilateral inverse-shell element with drilling degrees of freedom for shape sensing and structural health monitoring, Eng. Sci. Technol. an Int. J. 19 (2016) 1299–1313. https://doi.org/10.1016/j.jestch.2016.03.006.
- [3] P. Cerracchio, M. Gherlone, A. Tessler, Real-time displacement monitoring of a composite stiffened panel subjected to mechanical and thermal loads, Meccanica. 50 (2015) 2487–2496. https://doi.org/10.1007/s11012-015-0146-8.
- [4] E. Del Priore, L. Lampani, A methodology for applying isogeometric inverse finite element method to the shape sensing of stiffened thin-shell structures, Thin-Walled Struct. 199 (2024) 111837. https://doi.org/10.1016/j.tws.2024.111837.
- [5] M. Esposito, M. Mattone, M. Gherlone, Experimental Shape Sensing and Load Identification on a Stiffened Panel: A Comparative Study, Sensors. 22 (2022). https://doi.org/10.3390/s22031064.
- [6] D. Yu, S. Wang, W. Li, Y. Yang, J. Hong, Shape sensing for thin-shell spaceborne antennas with adaptive isogeometric analysis and inverse finite element method, Thin-Walled Struct. 192 (2023) 111154. https://doi.org/10.1016/j.tws.2023.111154.
- [7] M.A. Abdollahzadeh, H.Q. Ali, M. Yildiz, A. Kefal, Experimental and numerical investigation on large deformation reconstruction of thin laminated composite structures using inverse finite element method, Thin-Walled Struct. 178 (2022) 109485. https://doi.org/10.1016/j.tws.2022.109485.
- [8] L. Colombo, C. Sbarufatti, M. Giglio, Definition of a load adaptive baseline by inverse finite element method for structural damage identification, Mech. Syst. Signal Process. 120 (2019) 584–607. https://doi.org/10.1016/j.ymssp.2018.10.041.
- [9] D. Oboe, D. Poloni, C. Sbarufatti, M. Giglio, Crack Size Estimation with an Inverse Finite Element Model, in: Eur. Work. Struct. Heal. Monit. EWSHM 2022 Vol. 1, n.d. https://doi.org/https://doi.org/10.1007/978-3-031-07254-3.

1

IMPROVING SHAPE SENSING OF AERONAUTICAL STRUCTURES WITH SEA AND MOGA

- [10] A. Kefal, C. Diyaroglu, M. Yildiz, E. Oterkus, Coupling of peridynamics and inverse finite element method for shape sensing and crack propagation monitoring of plate structures, Comput. Methods Appl. Mech. Eng. 391 (2022) 114520. https://doi.org/10.1016/j.cma.2021.114520.
- [11] A. Tessler, H.R. Riggsb, C.E. Freesec, M. Cookd, An improved variational method for finite element stress recovery and a posteriori error estimation, Comput. Methods Appl. Mech. Eng. 7825 (1998). https://doi.org/https://doi.org/10.1016/S0045-7825(97)00135-7.
- [12] A. Kefal, I.E. Tabrizi, M. Yildiz, A. Tessler, A smoothed iFEM approach for efficient shape-sensing applications: Numerical and experimental validation on composite structures, Mech. Syst. Signal Process. 152 (2021) 107486. https://doi.org/10.1016/j.ymssp.2020.107486.
- [13] D. Oboe, L. Colombo, C. Sbarufatti, M. Giglio, Comparison of strain pre-extrapolation techniques for shape and strain sensing by iFEM of a composite plate subjected to compression buckling, Compos. Struct. 262 (2021) 113587. https://doi.org/10.1016/j.compstruct.2021.113587.
- [14] E. Del Priore, L. Lampani, Shape Sensing in Plate Structures through Inverse Finite Element Method Enhanced by Multi-Objective Genetic Optimization of Sensor Placement and Strain Pre-Extrapolation, Sensors. 24 (2024). https://doi.org/10.3390/s24020608.
- [15] K. Deb, A. Pratap, S. Agarwal, T. Meyarivan, A fast and elitist multiobjective genetic algorithm: NSGA-II, IEEE Trans. Evol. Comput. 6 (2002) 182–197. https://doi.org/10.1109/4235.996017.
- [16] A. Kefal, E. Oterkus, Displacement and stress monitoring of a Panamax containership using inverse finite element method, Ocean Eng. 119 (2016) 16–29. https://doi.org/10.1016/j.oceaneng.2016.04.025.
- [17] M. Gherlone, P. Cerracchio, M. Mattone, M. Di Sciuva, A. Tessler, Shape sensing of 3D frame structures using an inverse Finite Element Method, Int. J. Solids Struct. 49 (2012) 3100–3112. https://doi.org/10.1016/j.ijsolstr.2012.06.009.
- [18] A. Konak, D.W. Coit, A.E. Smith, Multi-objective optimization using genetic algorithms: A tutorial, Reliab. Eng. Syst. Saf. 91 (2006) 992–1007. https://doi.org/10.1016/j.ress.2005.11.018.
- [19] S. Wang, D. Zhao, J. Yuan, H. Li, Y. Gao, Application of NSGA-II Algorithm for fault diagnosis in power system, Electr. Power Syst. Res. 175 (2019) 105893. https://doi.org/10.1016/j.epsr.2019.105893.
- [20] A. Tessler, H.R. Riggs, M. Dambach, A novel four-node quadrilateral smoothing element for stress enhancement and error estimation, Int. J. Numer. Methods Eng. 44 (1999) 1527–1543. https://doi.org/10.1002/(SICI)1097-0207(19990410)44:10<1527::AID-NME497>3.0.CO;2-1.